Applied Thermal Engineering 226 (2023) 120268

Contents lists available at ScienceDirect

Applied Thermal Engineering

journal homepage: www.elsevier.com/locate/ate

Research Paper

A strategy to extend load operation map range in oxy-fuel compression ignition engines with oxygen separation membranes

F.J. Arnau *, G. Bracho, L.M. García-Cuevas, V.H. Farias

CMT Motores Térmicos, Universitat Politècnica de València, Spain

ARTICLE INFO

Keywords:
Oxy-fuel combustion
Internal combustion engine
Membrane
MIEC
Energy recovery
Carbon capture
Part-load

ABSTRACT

The possibility of applying oxy-fuel combustion to a compression ignition engine (CIE) at different operating points regarding engine speed and load is studied in this work. To do so, a strategy is proposed to extend the load operation map range of a 2.2 L turbocharged and direct-injection CIE under oxy-fuel combustion conditions using mixed ionic-electronic conducting membranes (MIEC) to acquire oxygen (O_2) from the air. As nitrogen is not present in the intake flow, nitrogen oxide (NO_x) emissions are eliminated, and carbon capture is allowed. The strategy consists of modifying exhaust gas temperature and oxygen-fuel ratio , generating temperature-lambda maps to decide the optimal combination in terms of engine performance. Thus, the system behavior is analyzed at three engine speeds (1250 rpm, 2500 rpm and 3500 rpm) with different load levels and compression ratio (CR) of 20. The baseline engine model is calibrated with experimental data within part-load operation ranges, and an apparent combustion time model calibrated with computational fluid dynamics data is applied to simulate the combustion process under oxy-fuel combustion conditions. Finally, specific parameters are researched to verify whether the system produces enough energy to heat up the MIEC, generating the necessary oxygen. Indeed, a few of them have been found very useful as design parameters for finding out oxy-fuel engine operation limits and estimating MIEC design features.

1. Introduction

At present, the effects of global warming have harmfully impacted environmental conditions worldwide as a consequence of an increase in greenhouse gas (GHG) emissions, especially carbon dioxide (CO_2), which is the primary long-lived GHG emitted from human activities in the atmosphere [1]. In this circumstance, the European Union (EU) has established ambitious goals for 2030, such as at least 32.5% improvement in process energy efficiency and at least 40% cuts in GHG [2] for 2030. Emissions of GHG from the EU's transport sector have steadily increased between 2013 and 2019, and road transport constitutes the most considerable amount of overall transport emissions (it emitted more than 70% of all domestic and international transport GHG in 2019) [3,4]. Therefore, solutions to mitigate the environmental footprint of road transport vehicles are claimed, such as synthesis of e-fuels (synthetic fuel with low environmental impact), vehicle adaptation to fuel-cell, hybrid electric and solar-powered arrangements, and development of systems with low or zero tank-to-wheel emissions [5–7]. In particular, current internal combustion engines (ICEs) represent almost 10% of worldwide pollutants from fossil fuels [8]. In this framework, oxy-fuel combustion arises as one of the most promising solutions to reduce and potentially eliminate GHG (CO_2) and air-deterioration pollutants emissions from combustion processes, among them unburnt hydrocarbons (HC), carbon monoxide (CO) and nitrogen oxides (NO_x).

Oxy-fuel combustion applied to ICE is a process in which the fuel is burnt with pure oxygen blended with exhaust gas recirculation (EGR) mainly composed by CO_2 and water vapor, instead of air [9]. Indeed, since in-chamber temperature achieved in pure-oxygen combustion could be much higher than in standard air operation, with an EGR-based dilution of oxygen, the engine thermo-mechanical limitations may be respected [10]. Moreover, once nitrogen is not present at intake gas, NO_x emissions may be entirely eliminated and the trade-off in combustion optimization between NOx and particle matter (PM) control disappears. Nowadays, oxy-fuel combustion is mainly mature in large-scale process such as power stations for generation of electric power burning fossil fuels (oil, coal and natural gas) [11,12] and biomass [13] in order to diminish CO_2 emissions. The oxy-fuel concept in combustors and furnaces has been widely investigated and recent progress has been reported. For example, Guo et al. presented a large-scale experimental study of oxy-fuel combustion and showed that this concept performs well with a special burner system designed for conditions with an initial O_2 concentration of 28% in the oxidant [14]. The influence of high CO_2 concentration has been evaluated in oxy-fuel plants for

* Corresponding author.
E-mail address: farnau@mot.upv.es (F.J. Arnau).

https://doi.org/10.1016/j.applthermaleng.2023.120268
Received 23 November 2022; Received in revised form 14 February 2023; Accepted 17 February 2023
Available online 28 February 2023

Nomenclature

Abbreviations

ACT	Apparent Combustion Time
BPV	Back Pressure Valve
BSFC	Brake Specific Fuel Consumption
CAD	Crank Degree Angle
CAS	Cryogenic Air Separation
CI	Compression Ignition
CR	Compression Ratio
CS	Control System
EGR	Exhaust Gas Recirculation
EU	European Union
GHG	Greenhouse Gas Emission
HE	Heat Exchanger
HEN	Heat Exchange Network
HRL	Heat Released Law
ICE	Internal Combustion Engine
MIEC	Mixed Ionic-Electronic Conducting Membrane
SC	Single Cylinder
SI	Spark Ignition
SOC	Start of Combustion
SOI	Start of Injection
VEMOD	Virtual Engine Model
VGT	Variable Geometry Turbocharger

Variables

$\dot{m}_{O_2}$	Mass flow of oxygen generated by the membrane
λ	Oxygen-fuel equivalence ratio
$H_{air,in,MIEC}$	Sensible enthalpy at MIEC feed side inlet
$H_{air,in,system}$	Sensible enthalpy at system air inlet
$H_{MIEC,real}$	Heat transferred to air from system entry until MIEC feed side inlet
HR	Heat released by combustion
Q_{C-1}	C-1 cooling power
Q_{htw}	Convective heat losses at cylinder walls
Q_{pipes}	Convective heat losses at exhaust pipes
T_{exh}	Exhaust gas temperature
$\dot{m}^*_{O_2}$	Mass flow of oxygen generated by membrane per engine cycle

different reaction temperatures and equivalence ratios [15]. In addition, the cement sector as well as the oil petroleum-refining industry are evaluating the feasibility of oxy-fuel combustion application on their operations [16,17]. Thus, that technology employed in ICE has a broad research field due to its novelty for enabling CO_2 capture from exhaust gas [18,19]. Once the exhaust stream essentially contains water vapor and CO_2, water may be easily separated through condensation at near-standard temperature and pressure conditions, and the remaining CO_2 may be pressurized through compression stages and stored in supercritical-fluid phase at ambient temperature [20].

In 2009, Osman et al. [21] proposed to apply the oxy-fuel concept to a single cylinder (SC) engine for the first time, injecting water and pure oxygen straightly into combustion chamber. They obtained an improvement in fuel-conversion efficiency reflected onto reduction in PM, CO, HC and NO_x emissions. Serrano et al. [22] evaluated the oxy-fuel technology in a SC spark-ignition (SI) engine through experimental and theoretical techniques considering thermal–mechanical constraints. They observed a decrease in indicated efficiency that may be balanced by knocking reduction, which fosters room for spark optimization with an EGR rate range from 60% to 70% to sustain combustion stability. Also, some works have arisen studying several variables for oxy-fuel combustion application to compression ignition (CI) engines such as varying the intake system oxygen concentration [23], water direct-injection parameters [24] and EGR [25], which means oxygen dilution, to find out reasonable flame temperature, control combustion stability and verify pollutant emissions mitigation. In addition, in part of those studies, the oxy-fuel process is coupled to some of well-known combustion concepts in ICE such as homogeneous charge compression ignition [9], internal combustion Rankine cycle [26] and closed-cycle diesel engine [27] to enhance power output and combustion efficiency while enabling carbon capture. However, most of those works found in the literature are carried out using SC engines and without considering oxygen generation, which is a key factor for contemplating the use of oxy-fuel combustion in non-stationary applications.

As already mentioned, one of the main worries of using that combustion in transport applications is the in-situ oxygen supply because, on the one hand, conventional oxygen generation systems like cryogenic air separation (CAS) are costly and energy-intensive [28]. On the other hand, onboard oxygen tanks would imply the need of oxygen refill, undermining vehicle autonomy, and lower indicated efficiency due to vehicle weight gain. In this context, mixed ionic-electronic conducting membranes (MIEC) may be considered as a promising solution to produce oxygen from the air without crucial economic- and energy penalties, being 10.5% to 17.5% more cost-effective than CAS with a power consumption abatement of 0.5% to 9% [29]. An oxygen partial pressure gradient between feed and permeate sides along with high temperature are the driving force for oxygen transport in those membranes [30]. Among different MIECs, $Ba_{0.5}Sr_{0.5}Co_{0.8}Fe_{0.2}O_{3-\delta}$ (BSCF) membranes have an elevated oxygen transfer rate generating up to $62\,mL\,min^{-1}\,cm^{-2}$ of oxygen at 1000 °C [31]. Indeed, Serra et al. [32] performed a characterization study of oxygen transport on MIEC BSCF through numerical and experimental evaluations, investigating the MIEC operation behavior varying some parameters such as feeding flow, MIEC temperature, sweep gas composition (oxygen dilution with H_2O, CO_2, Ar or He) and sweep inlet flow. Although CO_2 may jeopardize BSCF membrane performance, there are meaningful progresses in developing protective layers such as $Ce_{0.9}Gd_{0.1}O_{2-\delta}$ films which may be deposited on those membranes to improve their stability under CO_2-containing environments [33,34]. The outcomes of their work indicate that an improvement in oxygen production is achieved when the BSCF MIEC is submitted to temperatures from 700 °C to 1000 °C and when H_2O or CO_2 are used as a sweep gas for reducing the oxygen partial pressure at permeate side. Thus, BSCF membranes appear as a reasonable approach for in-situ oxygen separation in ICE using the flue gas as a sweep gas at permeate side and exploiting its waste heat to produce enough temperature and pressure on MIEC feed side to generate the oxygen which is necessary for proper engine operation under oxy-fuel combustion environment as patented by Desantes et al. [35].

This paper aims to continue the study developed by Serrano et al. [36] wherein the oxy-fuel combustion is applied to a CIE over the full speed-load range using an oxygen supply system based on MIEC technology. Therefore, this second part intends to extend the engine operating map towards part-load conditions assessing the system performance in oxy-fuel combustion mode. To do so, the regenerative cycle layout built in previous work, as well as the BSCF MIEC model based on results obtained by Serra et al. [32] for oxygen production are maintained, and the EGR control system 1 depicted in that work is considered to propose a strategy to lower the engine load controlling the amount of injected fuel combining the following approaches:

- The first approach consists of working with a constant oxygen-fuel ratio (λ), lowering the exhaust gas temperature (T_{exh}) and, thereby, decreasing the MIEC oxygen production capacity.

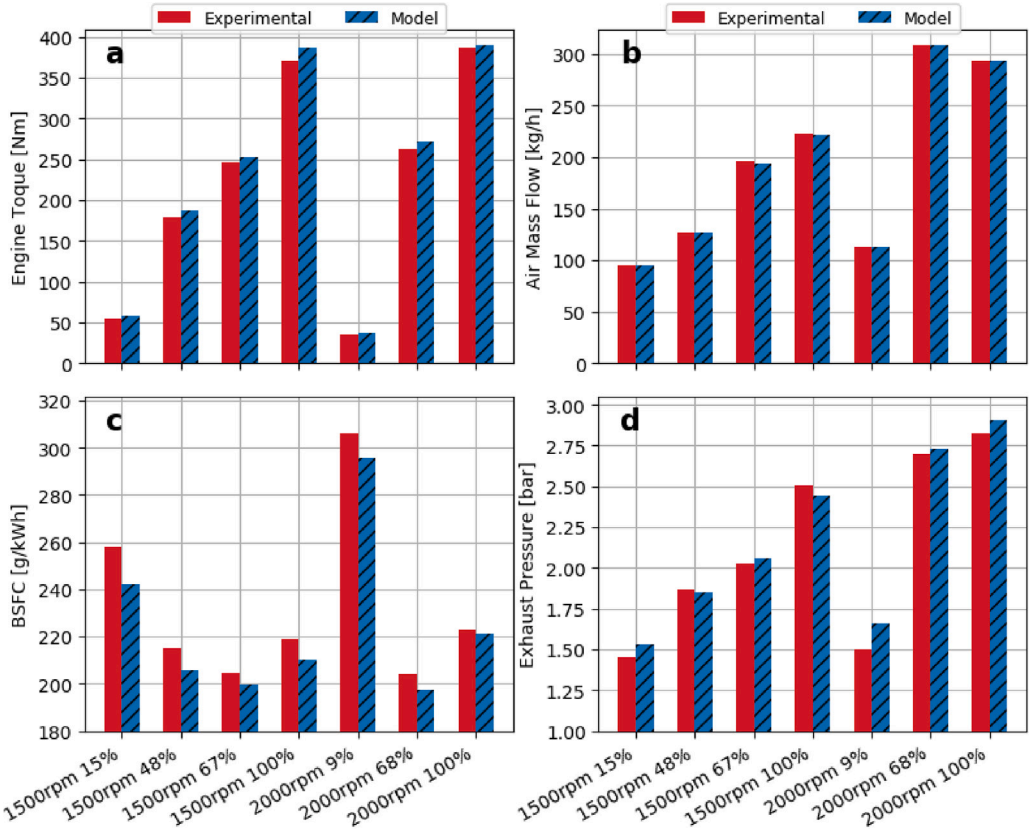

Fig. 1. Comparison between experimental and simulation data for the baseline turbocharged IC standard air engine considering various load levels for two engine speeds. (a) Engine torque; (b) Air mass flow entering the cylinders; (c) Brake specific fuel consumption (BSFC); (d) Exhaust manifold pressure.

- The second approach is based on keeping T_{exh} constant while the load is reduced by decreasing the amount of injected fuel.

For this paper, a combustion reduced order model is applied under the oxy-fuel conditions. Indeed, that model uses the apparent combustion time (ACT) characteristic of a diffusion combustion process to find out clear relations between the rate of heat release, in-cylinder conditions (oxygen concentration, air density, ...) and the injection rate law [37,38]. As shown by Arregle et al. [39], a genetic algorithm adjusts some constants of the model with experimental data from several engines, and the model validation is based on a vast range of tested engines with different operating conditions. Finally, to the best of the authors' knowledge, this is the first work proposing methods to decrease the load in ICEs with onboard self-generation of oxygen utilizing MIECs for enabling carbon capture from the exhaust gas.

The manuscript is structured as follows: first, the model is described in Section 2; then, the results are presented and discussed in Section 3; finally, Section 4 includes the main conclusions of this work.

2. Methodology

The models employed in this study are built up and implemented into Virtual Engine Model (VEMOD), an in-house and non-commercial gas-dynamic software that researchers have developed at CMT – Motores Térmicos [40]. There is a wide range of sub-models inside VEMOD to simulate elements such as EGR and air-charge coolers, turbocharging and after-treatment systems, throttle valves, and 0D MIEC model, taking into account 1D gas dynamics and heat transfer, including gas-to-wall heat exchange and wall temperature prediction. Therefore, all those cited sub-models are embedded into VEMOD to calculate thermo and fluid dynamic processes in ICEs for transient and steady-state cases within vast operating range [41].

The same 2.2 L turbocharged and direct injection CIE used as a baseline for modeling the oxy-fuel engine considering the full-load operation depicted by Serrano et al. [36] is utilized in this work. In addition, Fig. 1 shows how part-load points are reasonably calibrated, indicating that the VEMOD model is still valid to simulate the same baseline engine within a broader operating range. Also, the benchmark engine optimized model calibrated in that previous article is preserved as well as the sub-models of auxiliary elements composing the oxy-fuel layout such as variable geometry turbocharger (VGT), heat exchangers (HEs) and gas flow regulation components (valves, plenums, and pipes). In particular, the combustion chamber geometry and injection system are deeply optimized considering the computational fluid dynamics (CFD) outputs presented by Serrano et al. [42] in their study of a SC CIE in oxy-fuel combustion mode. Some heat-exchanger and turbocharge layouts were previously proposed in patent [35]. However, the optimized one in terms of engine efficiency, energy recovery and packaging presented in that previous paper is still contemplated maintaining the EGR CS 1 described in [36] as starting point to study methods to reduce the engine load as shown in Fig. 2.

In the layout, the different fluids are described as follows:

- The orange line represents the fuel flow.
- The black line represents air flow.
- The green line represents a nitrogen-enriched flow.
- The red line represents the exhaust gas flow composed mainly by CO_2 and water.
- The blue line, also called oxidizer line, represents a blend composed by O_2, CO_2 and water which enters the cylinders.

A regenerative Brayton cycle is composed of the black and green lines with intermediate reheating and cooling between expansion and compression stages, respectively, to produce high temperature and pressure on the MIEC feeding side. The combustion chamber present

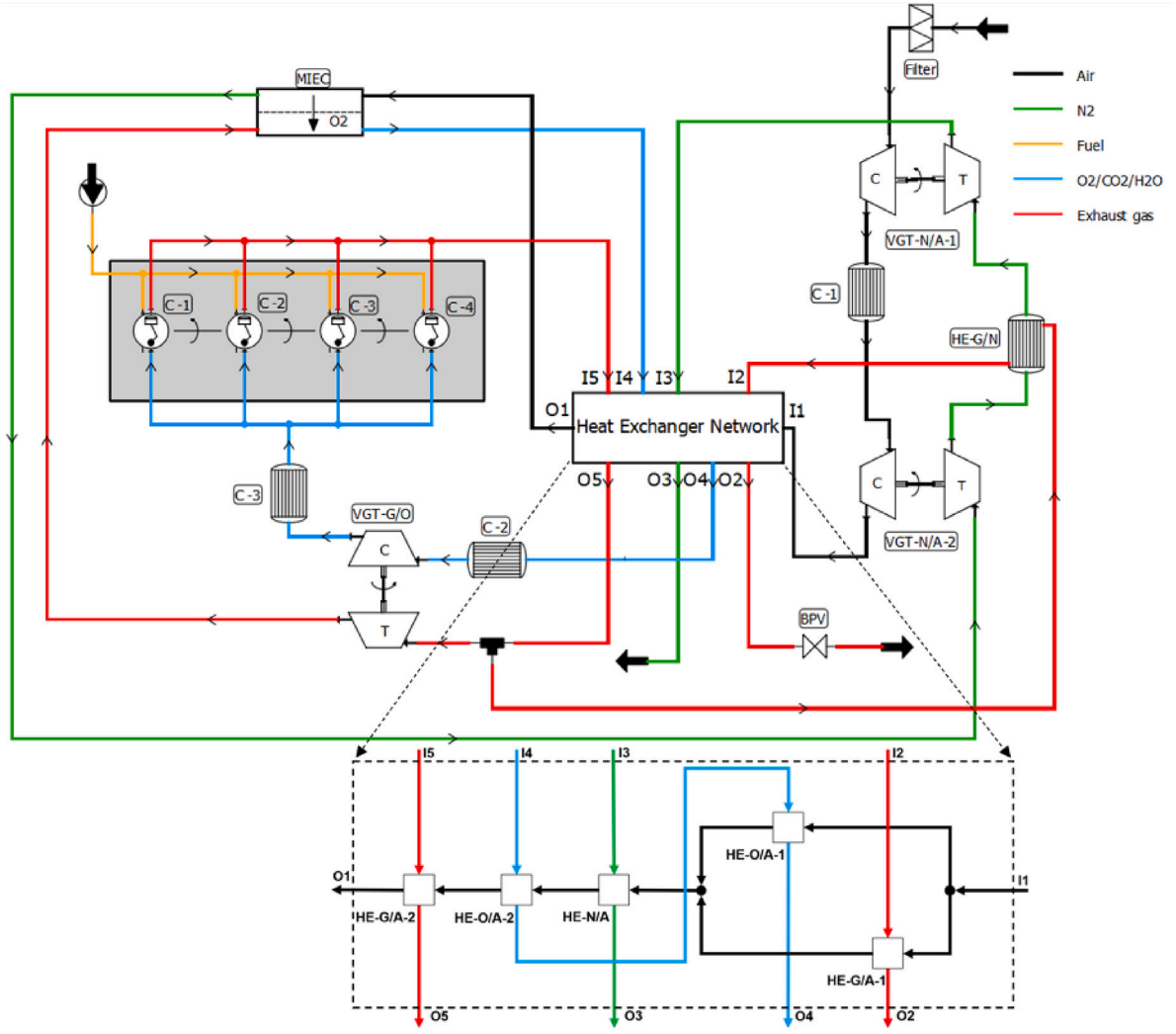

Fig. 2. Layout of the oxy-fuel combustion concept.

in conventional Brayton cycles is replaced by the MIEC, which is the connecting point between the CIE cycle and the regenerative Brayton cycle. In order to facilitate the carbon capture and raise the intake gas density, regeneration is used to cool down the $CO_2 + H_2O$ and oxidizer lines and recovers pressurizing energy from the nitrogen-enriched line. Therefore, the regenerative Brayon is composed of several HEs arranged along the airflow line to rise MIEC feeding side temperature up to around 900 °C retrieving part of exhaust gas wasted energy, and two turbochargers in series at system inlet to compress air up to around 5 bar.

Air is pressurized by two compression stages with inter-cooling and heated up by a Heat Exchanger Network (HEN) (Fig. 2). Cooler C-1 improves compression efficiency lowering VGT-NA-2 compressor inlet temperature and avoiding hazardous operation. Two HEs in parallel followed by three HEs in series form the HEN: HE O/A-1 and HE O/A-2 increase air temperature cooling down the oxidizer line. HE G/A-1 and HE G/A-2 recover exhaust gas wasted energy, and when HE O/A-1 and HE G/A-1 are not able to supply enough heat, HE N/A is convenient for warming up the air with residual thermal energy at nitrogen line. The nitrogen which leaves the MIEC passes through two expansion stages with intermediate reheating converting its thermal energy into compression power to pressurize air coming from the ambient. Finally, HE G/N transfers heat from flue gas to nitrogen, enhancing VGT NA-1 performance due to an increment of its inlet temperature (Fig. 2).

EGR reduces oxygen partial pressure at the permeate side by diluting the oxygen transferred from MIEC, improving oxygen production,

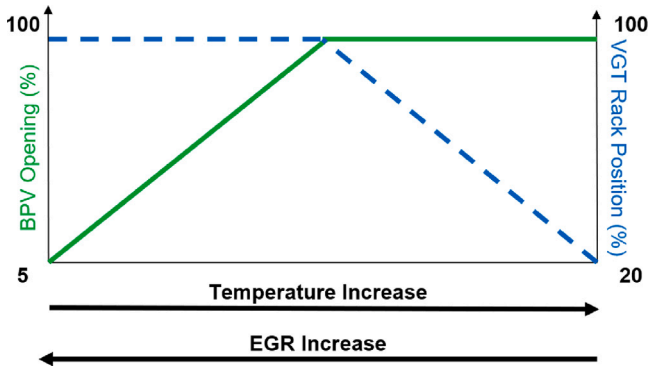

Fig. 3. Exhaust manifold temperature control.

and maintaining combustion and cylinder outlet temperatures. Oxidizer flow supplies heat to the air via HE O/A-1 and HE O/A-2 and is cooled down by coolers C-2 and C-3 at VGT GO compressor and cylinder inlets, respectively, so as to rise intake gas density and, thereby, enhancing its volumetric efficiency. The cylinder outflow gas heats up MIEC inlet air at HE G/A-2 and is separated into system-out exhaust gas and EGR. On the one hand, system-out flue gas transfers thermal energy to regenerative Brayton cycle through HE G/N and HEN. Besided, to lower

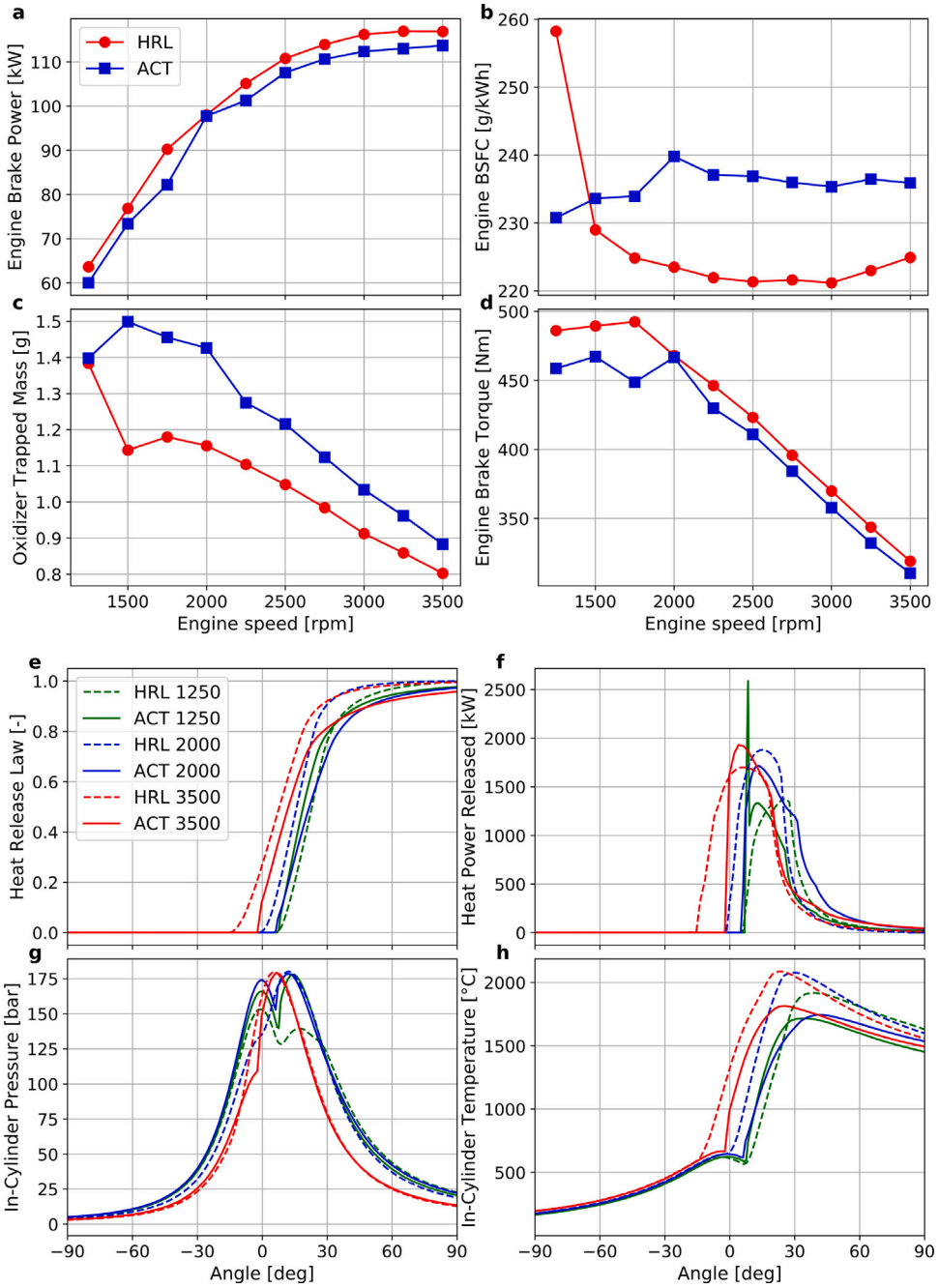

Fig. 4. Full-load curve average results of relevant engine variables with CR = 28 and for both combustion models (a, b, c and d). Instantaneous results of in-cylinder parameters at 1250 rpm, 2000 rpm and 3500 rpm at full load with CR = 28 for both combustion models (e, f, g and h).

MIEC permeate side pressure, EGR flow is submitted to an expansion at the VGT GO turbine. In addition, the T_{exh} is controlled by a back-pressure valve (BPV) coupled to the VGT GO turbine position, which is explained in Section 2.1.

2.1. Brief model description

As mentioned above, ACT is used in this study to simulate the combustion behavior for predicting the start of combustion (SOC) and heat power released, taking into account premixed and diffusion zones. In this case, that model was calibrated and validated by Arregle and al. [37–39] testing several engines at various operating situations. Moreover, it has been calibrated with CFD simulation data obtained by Serrano et al. [42] for an oxy-fuel combustion SC CIE with the same geometry, fuel, and injection system as the one used in this work. The ACT model has been adjusted based on a wide parametric study using results presented in [42]. The tuning of the model has been made to consider the larger specific heat capacity of the carbon dioxide molecule compared with oxygen and nitrogen (the dominant parts of the air). An increment of CO_2 in the combustion chamber (maintaining the same intake temperature and pressure) will vary the specific heat capacity of the mixture causing a lower temperature rise, and a larger ignition delay period in the combustion phase.

As depicted in Fig. 3, which presents the temperature control strategy, when ICE needs less combustion temperature, cylinder inlet oxygen concentration must be reduced by increasing EGR rate. Thus, in that case, since VGT GO turbine is operated as throttling valve at quasi-shock circumstance, its rack position is gradually open to raise EGR

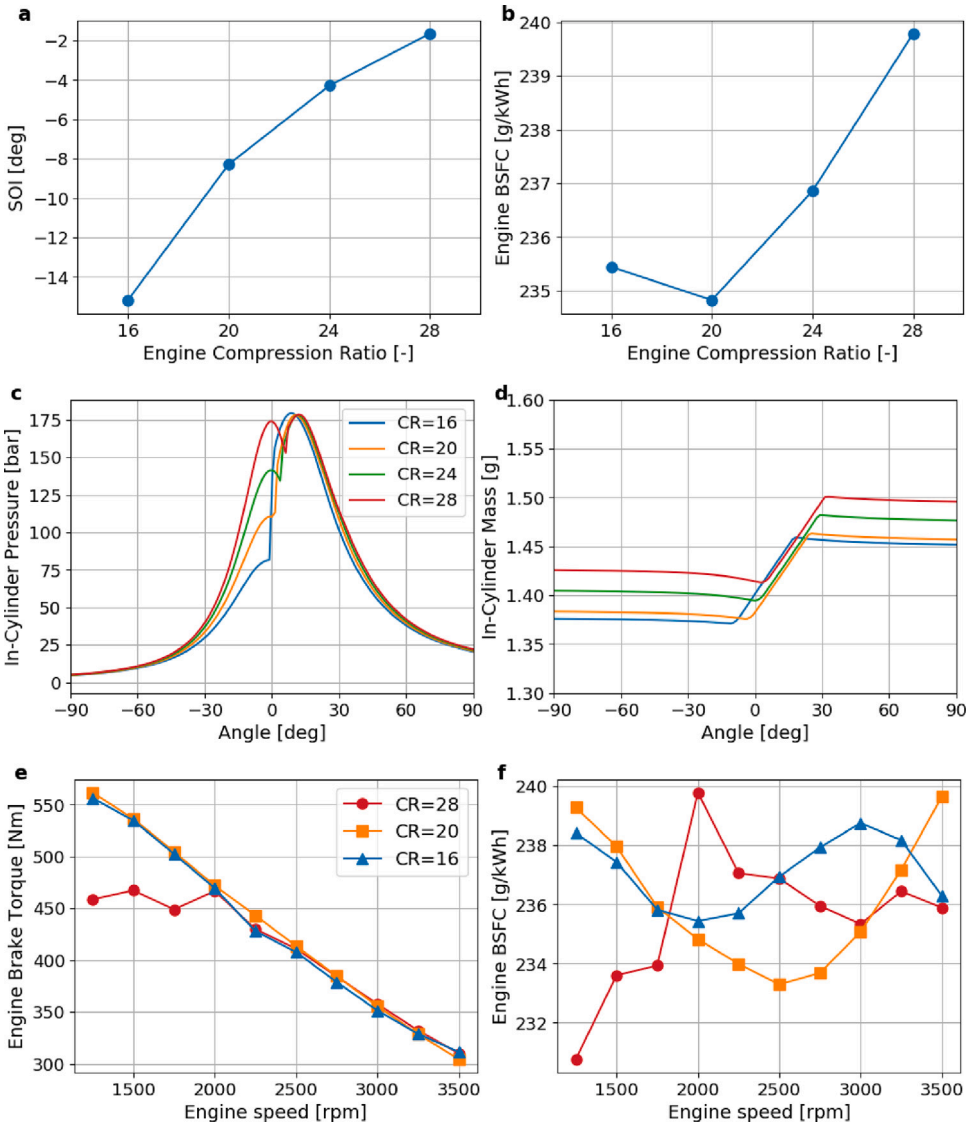

Fig. 5. Average results for CR curve at 2000 rpm (a and b). Instantaneous results for different CRs at 2000 rpm (c and d). Full-load curve average results for different CRs (e and f).

keeping BPV at its maximum lift (100%), and once rack has achieved its upper limit (100%), BPV lift is progressively closed rising intake CO_2 dilution. In this regard, the minimum values for BPV and turbine rack are 5% and 20%, respectively.

For all studies carried out in this work, the membrane surface is fixed at 10 m^2 and the cooler C-3 model is operated to keep a 85 °C cylinder intake temperature in order to avoid in-cylinder water condensation. Detailed information about HE, turbocharger, and MIEC models, as well as procedures for their sizing and optimization is available in [36].

2.2. Compression ratio (CR) study

As a starting point, the engine full-load curve from 1250 rpm to 3500 rpm is built up taking into account ACT as combustion model and CR = 28. Actually, that value is found by Serrano et al. [36] after a geometry assessment for the same multi-cylinder engine employed in this work, but using a heat released law (HRL) as the combustion model. Therefore, the start of injection (SOI) is submitted to an optimization process with constrains (T_{exh} = 1000 °C and Maximum In-cylinder Pressure ≤ 180 bar) to maximize torque and engine efficiency as depicted in Eq. (1). Fig. 4 shows a comparison in terms of average and instantaneous results between ACT and HRL combustion model, which was imposed to perform calculations by Serrano et al. with gasoil [36]. For both cases, λ = 1.1 is held.

$$\max_{soc} \quad \text{ObjectiveFunction}(soc) = \text{Efficiency}(soc) \times \text{Torque}(soc) \tag{1}$$

If compared to imposed diesel HRL outputs, engine brake power using ACT model adapted to oxy-fuel combustion is slightly lower (Fig. 4a), and its BSFC is mainly more elevated at high-intermediate engine speeds (on average, more than 7%) (Fig. 4b) due to significant unburnt fuel (around 5%) present at the end of combustion phase (Fig. 4a). That issue is not observed using the HRL model due to its assumption of complete fuel burn. Indeed, as oxy-fuel combustion modeled with ACT has a peak of heat release at SOC (Fig. 4b), which is not seen in conventional combustion, SOI must be delayed not to surpass maximum in-cylinder pressure (Fig. 4c). In that case, BPV must be closer which entails more in-chamber trapped mass (Fig. 4d) to control combustion temperature (Fig. 4d). Furthermore, from 1250 rpm to 2000 rpm the engine brake torque is relatively constant for ACT (Fig. 4c) because in-cylinder maximum pressure is almost reached only with compression phase and, thereby, exhaust temperature had to be reduced from 1000 °C to 925 °C so as to fulfill the pressure constrain. In fact, 925 °C is the maximum exhaust temperature allowed within that engine speed range wherein in-chamber maximum pressure may

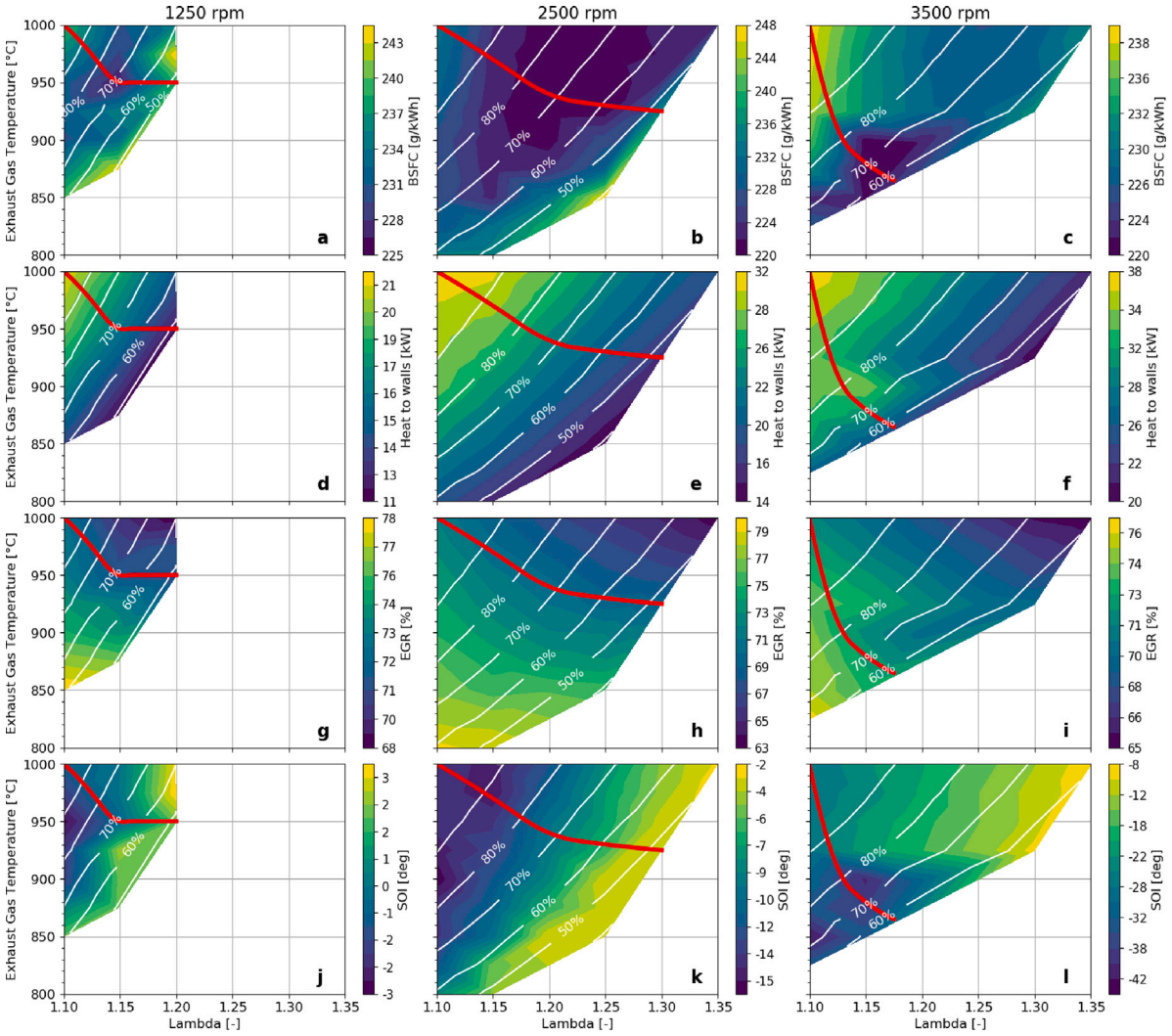

Fig. 6. Part-load maps for average results of relevant engine variables for 1250 rpm, 2500 rpm and 3500 rpm. The white lines drawn on maps represent level curve for degree of engine load relative to maximum power achieved at corresponding engine speed.

be lesser or equal than 180 bar and, consequently, that suggests that CR should be reduced (Fig. 4c).

Thus, a study of CR is carried out at 2000 rpm, that is the maximum-torque engine speed, wherein compression stage pressure peak begins to be around 180 bar. In this regard, other variables are held constant, and SOI is optimized as already described. As shown in Fig. 5, with lower CR there is more room to bring forward SOI (Fig. 5a) without exceeding pressure constrain (Fig. 5C). At high CRs, the compression process already achieves elevated pressures, forcing SOI delay and increasing BSFC. In addition, more delayed SOI implies more EGR to control T_{exh}, which is reflected on more trapped mass (Fig. 5d), and a minimum BSFC is reached with CR = 20 (Fig. 5b). Likewise, to conclude this study, a full-load curve is generated optimizing SOI and taking into account three CRs of interest: 16 (engine baseline original CR), 28 (best CR found in [36,42]), and 20 (optimum CR at 2000 rpm). Also, calculations for CR = 16 and CR = 20 could be performed using T_{exh} = 1000 °C, not imposing a limitation on torque improvement from 1250 rpm to 1750 rpm (Fig. 5e). In addition, as shown in Fig. 5f, CR = 20 appears to have slightly better effective efficiency in general, especially within intermediate engine speeds and, thereby, authors consider that value satisfactory to be set for carrying out all calculations from high to low engine loads.

3. Results and discussion

As mentioned before, the strategy to extend the engine map towards part-load conditions at fixed rotation speed is based on combining two approaches, generating a vast amount of operating points. The first one is based on operating the system with less T_{exh} at constant λ, decreasing MIEC thermal energy and, consequently, oxygen generation, which results in less injected fuel. Furthermore, in-cylinder convective heat losses may be reduced with lower T_{exh}. The second approach maintains T_{exh} constant at any value, and λ is increased by decreasing the amount of injected, leading to less brake power. In the latter situation, combustion may be enhanced due to more in-chamber oxygen enrichment at the cost of "wasting" unused oxygen produced at MIEC. Accordingly, the objective is to look for the optimum combination of both approaches regarding engine minimum consumption. Finally, the optimization method outlined in Eq. (1) is also applied for each combination of actions, and some indicators are proposed to analyze limitations encountered to lower power at a given engine speed.

Therefore, in this section, part-load average result maps and instantaneous outputs for 1250 rpm, 2500 rpm and 3500 rpm are analyzed (Section 3.1); temperature, pressure and mass flow diagrams for highest and lowest brake power at 2500 rpm are compared (Section 3.2); and part-load limit indexes are discussed (Section 3.3).

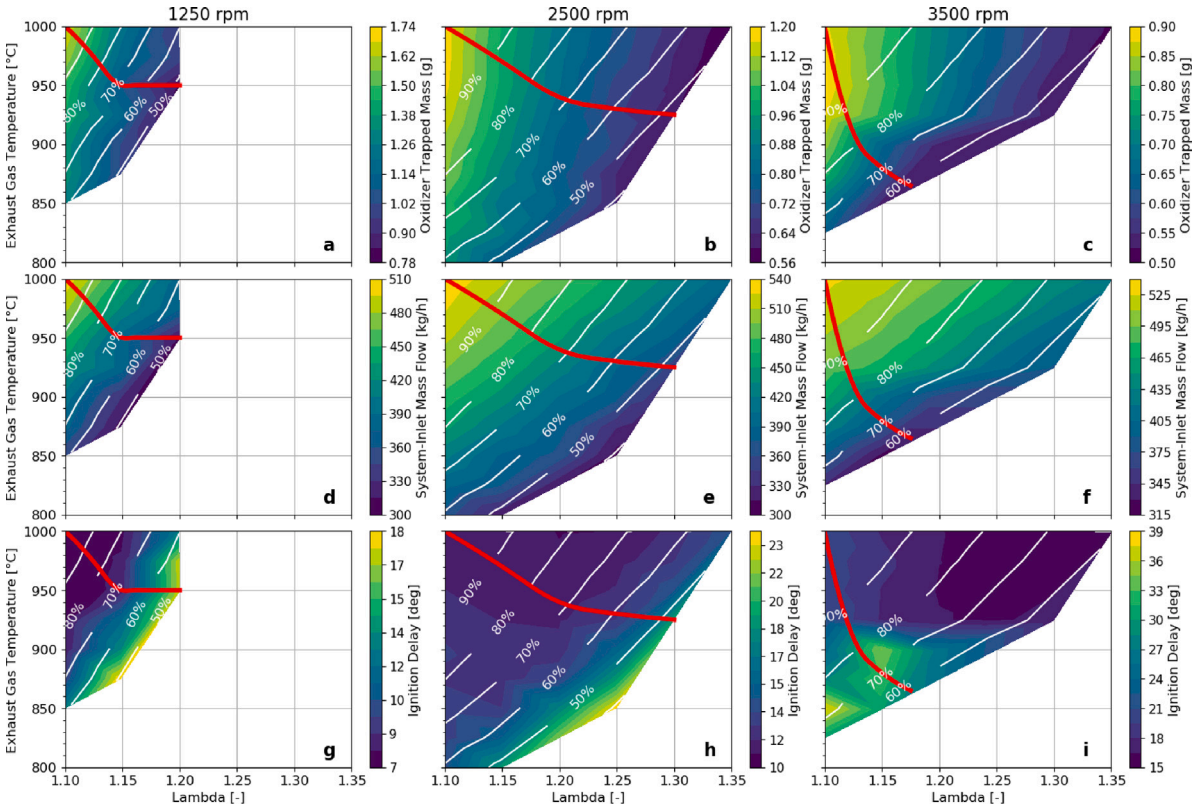

Fig. 7. Part-load maps for average results of relevant engine variables for 1250 rpm, 2500 rpm and 3500 rpm. The white lines drawn on maps represent level curve for degree of engine load relative to maximum power achieved at corresponding engine speed.

3.1. Average and instantaneous results and turbocharger maps

In Figs. 6–8 x-axis represents λ and y-axis T_{exh}. White lines represent the percentage of engine load as shown on color maps. As may be seen, the full-load point would be located in the upper-left corner and would correspond to the operating point with the highest T_{exh} = 1000 °C and the lowest λ = 1.1. As these simulations are very time-consuming, the points of T_{exh} and λ are created with discrete intervals of 25 °C and 0.05 respectively without impairing data analysis accuracy.

As depicted in Fig. 6a–c, there is a sort of minimum consumption zone due to low exhaust temperatures, with less convective heat losses (Fig. 6d–f), coupled to excess of oxygen, that enhances combustion performance. BSFC values down to 220 g/kWh are reached for 2500 rpm and 3500 rpm and 225 g/kWh for 1250 rpm. Actually, the best effective-efficiency temperature-lambda paths are present as the red lines in Figs. 6–8 for different engine speeds. In addition, when Fig. 6a–c is contrasted with Fig. 6g–i, the red lines similarly follow iso-EGR trends, indicating that an increase in λ should be followed by around 71% to 73% EGR rate in order to reduce engine load optimally.

Also, SOI must be delayed (Fig. 6j–l) mainly at a fixed temperature so as to provide more energy for exhaust gas in favor of keeping MIEC thermal requirements for oxygen generation at the cost of less mechanical power. Indeed, if SOI is delayed, more sensible enthalpy is available at the exhaust gas. Accordingly, more energy may be transferred to system inlet air via HEs in order to heat up the MIEC feed side for oxygen production. In addition, more λ entails more production of useless oxygen; however, that may reduce combustion-end HCs due to more in-chamber oxygen availability. In general, low engine speed points have SOI more delayed in order to center combustion. As expected, increasing inerts recirculation (Fig. 6g–i) decreases cylinder-out temperature since inert gas may absorb a substantial part of heat power released. The reverse effect is seen, though to a lesser extent, when intake gases are diluted with an excess of oxygen increasing λ and less EGR is required to control combustion temperature. Despite the EGR behavior being quite similar in all engine speeds, more oxidizer trapped mass is observed at low engine speeds due to more in-cylinder gas residence time (Fig. 7a–c). As this research is mainly focused on proposing minimum-consumption temperature-lambda paths for lowering engine load, only three engine speeds are contemplated in this study. However, the same process may be carried out for other engine speeds to find out their corresponding effective-efficiency paths and extend the engine part-load operating range.

When the engine load is reduced, less sensible enthalpy is available in the exhaust line, reflecting on less energy for the regenerative Brayton cycle and, consequently, depletion of system-inlet air mass flow (Fig. 7d–f). In this case, less oxygen is produced by the MIEC (Fig. 8a–c), diminishing oxidizer trapped mass. Although oxygen partial pressure ratio increases with less T_{exh} due to lower oxygen concentration at MIEC permeate side with more EGR rate (Fig. 8d–f), MIEC filtration capacity decreases with engine load reduction (Fig. 8g–i). Indeed, a decrease in the exhaust gas heat availability lowers MIEC feed side temperature and, thereby, harms membrane filtration.

Fig. 9 shows some in-cylinder variable instantaneous results for a particular engine speed = 2500 rpm which is taken for the sake of simplicity, the same trends may be observed at other engine speeds. As depicted in Fig. 9a–c, in-cylinder maximum pressure varies from 180 bar to 75 bar when λ increases and T_{exh} is reduced for lowering load. Also, when λ increases, the sudden rise in pressure at SOC is delayed and the pressure during compression phase is lower due to less trapped mass and need of more energy at exhaust gas, moving SOI towards ascending crank angle degree (CAD). In particular, ignition pressure is reduced, though to a lesser degree, lowering exhaust temperature and, apparently, a required minimum pressure is observed (around 40 bar) whereby combustion may be ignited regardless of λ and exhaust temperature, setting limits of feasible combustion. Fig. 9d–f shows that the maximum combustion temperature increases with more λ due to

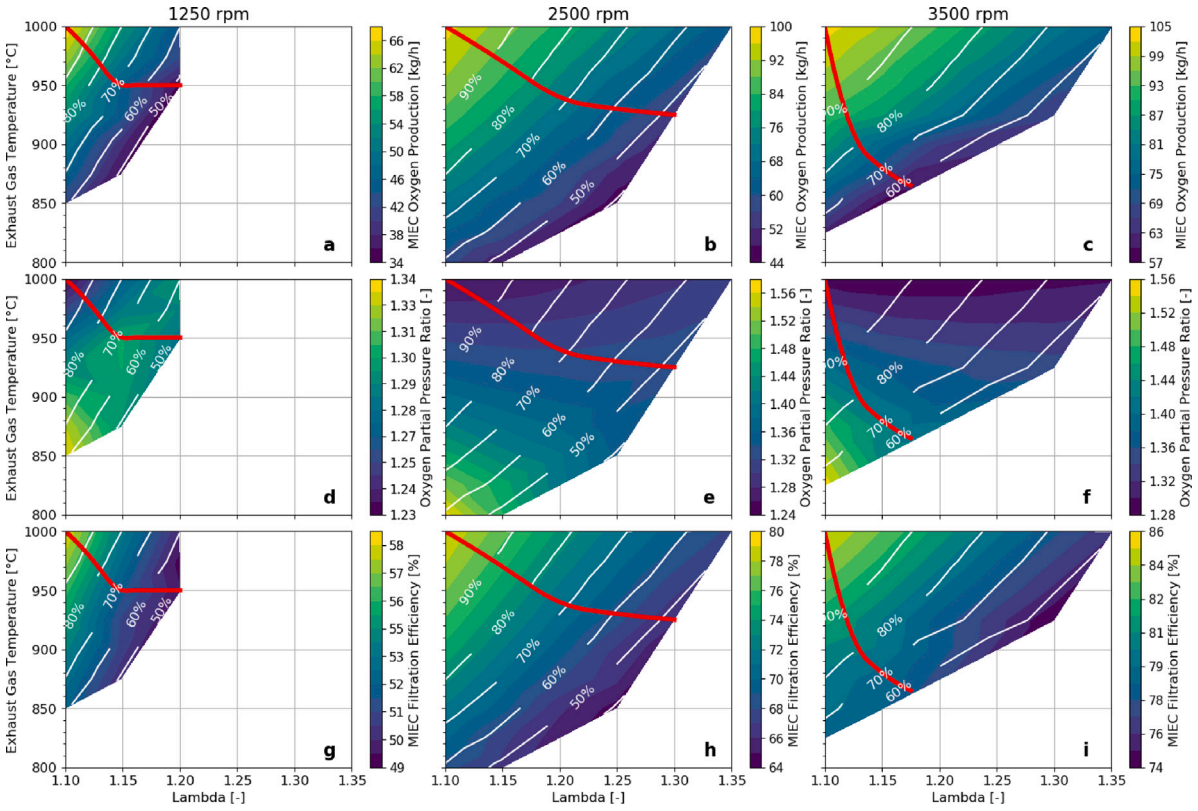

Fig. 8. Part-load maps for average results of relevant MIEC variables for 1250 rpm, 2500 rpm and 3500 rpm. The white lines drawn on maps represent level curve for degree of engine load relative to maximum power achieved at corresponding engine speed.

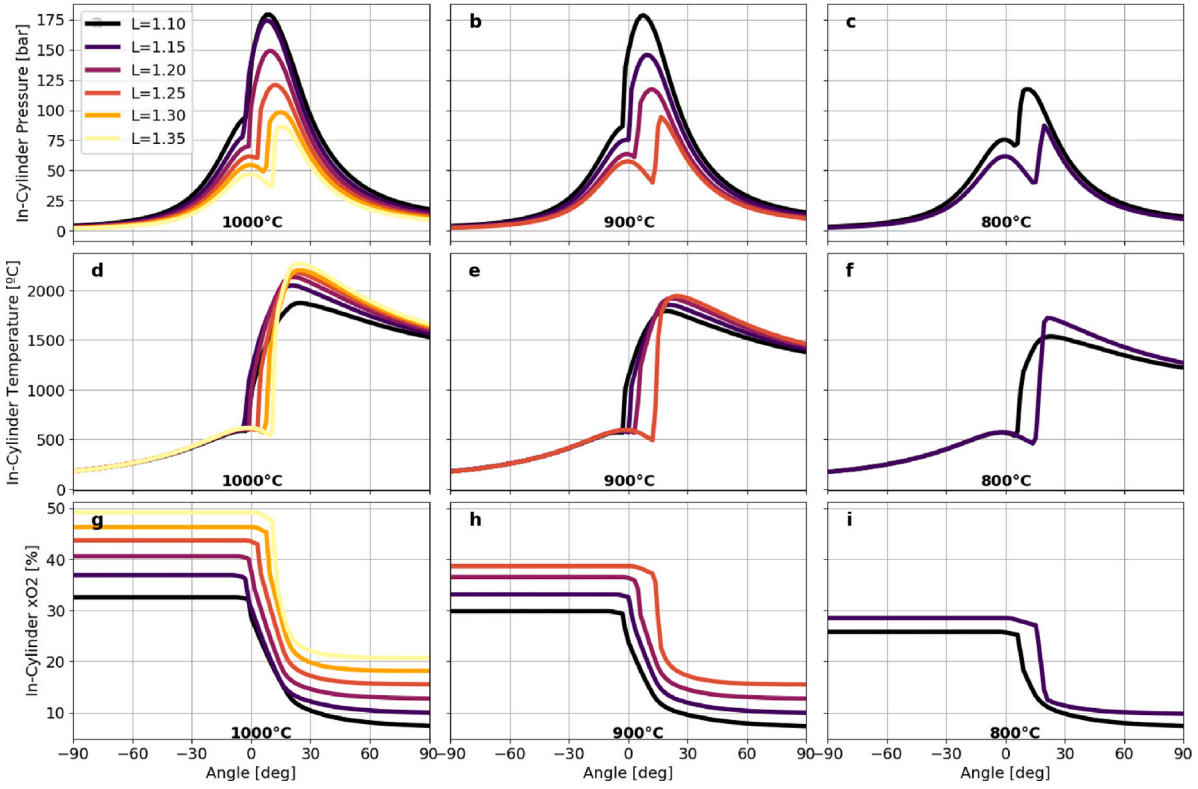

Fig. 9. In-cylinder variable instantaneous results at fixed engine speed = 2500 rpm for different values of T_{exh} (1000 °C, 900 °C and 800 °C). x_{O2} represents oxygen mass fraction.

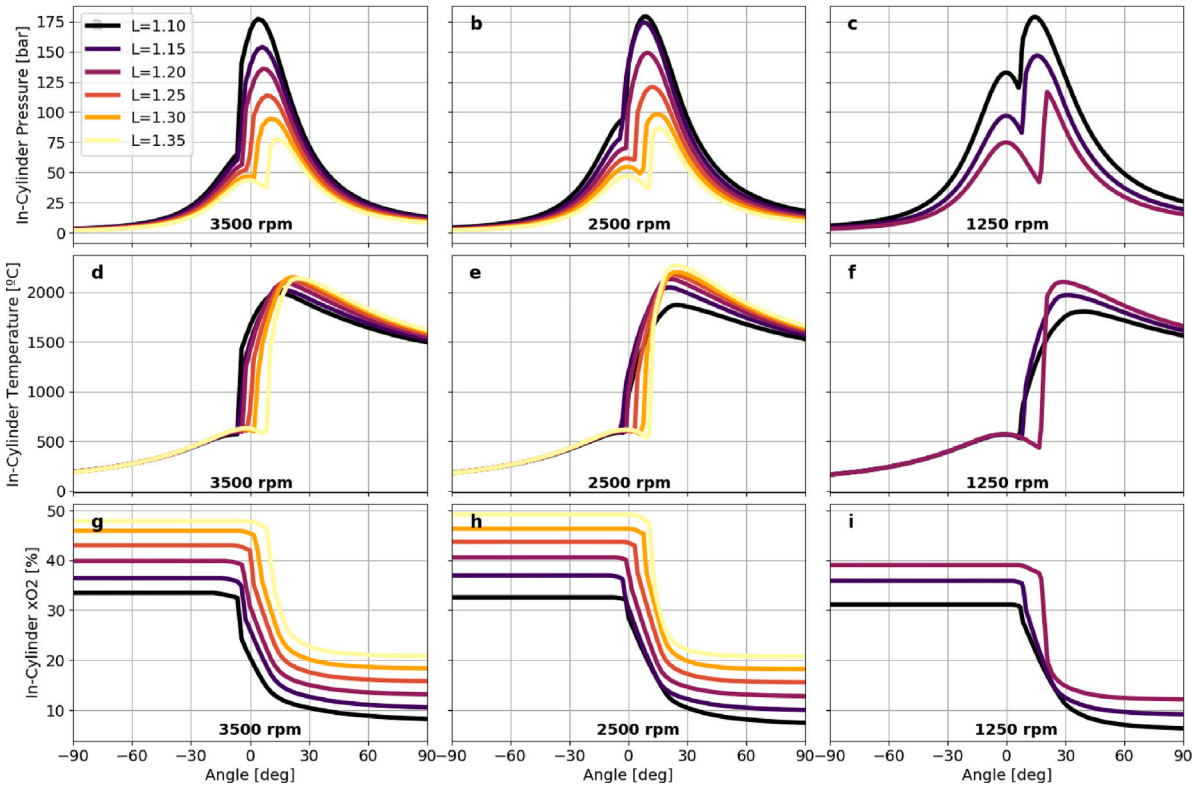

Fig. 10. In-cylinder variable instantaneous results at constant T_{exh} = 1000 °C for different values of engine speeds (3500 rpm, 2500 rpm and 1250 rpm). x_{O2} represents oxygen mass fraction.

combustion decentralization caused by SOI delay. Moreover, if Fig. 6g–i is compared to Fig. 9d–f, when λ increases, the ignition delay may be longer or shorter depending on conditions change. Thus, if the ignition time is too long, the fuel is burnt during the premixed phase and, hence, the combustion process is sharper. Nevertheless, ignition temperature seems to be around 550 °C for all engine speeds and part-load points with more dependence on SOI. As expected, more λ raises in-cylinder oxygen concentration that is reduced with lower exhaust temperature at constant λ due to less oxygen production (Fig. 9g–i). Although more λ entails more oxygen availability, that is not enough to trigger combustion if the in-cylinder pressure is not suitable, as already explained.

Fig. 10 presents similar trends to those depicted in Fig. 9, varying engine speed at constant T_{exh} = 1000 °C. In this case, maximum pressure Fig. 10a–c, maximum temperature Fig. 10d–f and oxygen concentration Fig. 10g–i have relatively same values, varying engine speed at fixed λ. Furthermore, SOI must be advanced at high engine speeds so as to center the combustion properly (Fig. 6e–f), which is seen comparing instantaneous (Fig. 10a–c) results for 3500 rpm, 2500 rpm and 1250 rpm at same λ and T_{exh}. Thus, once SOI is very advanced at 3500 rpm, the combustion ignition usually takes place during compression phase with high ignition pressure (Fig. 10a) and, hence, ignition delay decreases when load is reduced at T_{exh} = 1000 °C increasing λ (Fig. 6f and i). However, a reverse effect is seen for 2500 rpm and 1250 rpm because combustion usually occurs after 0 CAD when in-cylinder pressure is already decreasing (Fig. 10b and c) and, thereby, ignition time increases due to SOI delay (Fig. 6d, e, g and h).

Regarding the Brayton cycle compressors, they present their full-load operating points reunited nearby maximum efficiency zones with compression ratios from 2.0 to 3.5 (Fig. 11a and c). Also, their turbines operate with a suited expansion ratio from 1.5 to 3.0 at VGT position = 60% (Fig. 11b and d). Nonetheless, when engine load decreases, less energy is available at turbines (expansion ratio is reduced primary for VGT NA-1), and independently of engine speed, air compressors tend to be operated with lower compression ratios (minimum value reached around 1.7) and with worse efficiencies. Concerning VGT GO, the exhaust temperature is mainly controlled by the back pressure valve in all part-load points regardless of engine speed because its turbine is continuously operated at maximum rack position with low compression- and expansion ratios.

3.2. Temperature, pressure and mass flow diagrams

Fig. 12 presents temperature and power diagram for highest and lowest engine loads at 2500 rpm which is an intermediate speed for the sake of analysis. That part-load point corresponds to T_{exh} = 850 °C and λ = 1.25 where load is around 40% if compared to full-load point at same engine speed. Calculated temperatures are shown next to each flow line in degrees Celsius, with bottom values for low load and top ones for high load. Furthermore, heat power exchanged between fluids is depicted next to coolers and HEs in kW following the same temperature arrangement. That analogous representation scheme is also employed on pressure and mass flow diagrams (Figs. 13 and 14).

Low load point possess lower heat exchanged, implying colder fluids due to less energy produced in the combustion chamber, reflecting on less exhaust gas heat. In fact, some heat exchangers present power reduction of up to around 50% and 70% for HEs and coolers, respectively. In addition, as this system is based on a regenerative process, that cut in energy availability may also justify pressure and mass flow declines (Figs. 13 and 14) since nitrogen VGTs may no longer supply enough air to generate high pressure at MIEC feed side for oxygen production. Indeed, pressure and mass flow are reduced by half in general. One may see that more oxygen content is seen in the exhaust gas at low engine load as a consequence of working with more λ.

3.3. Part-load limit analysis indicators

With the purpose of analyzing the system energy performance within different operating conditions, some variables must be indicated

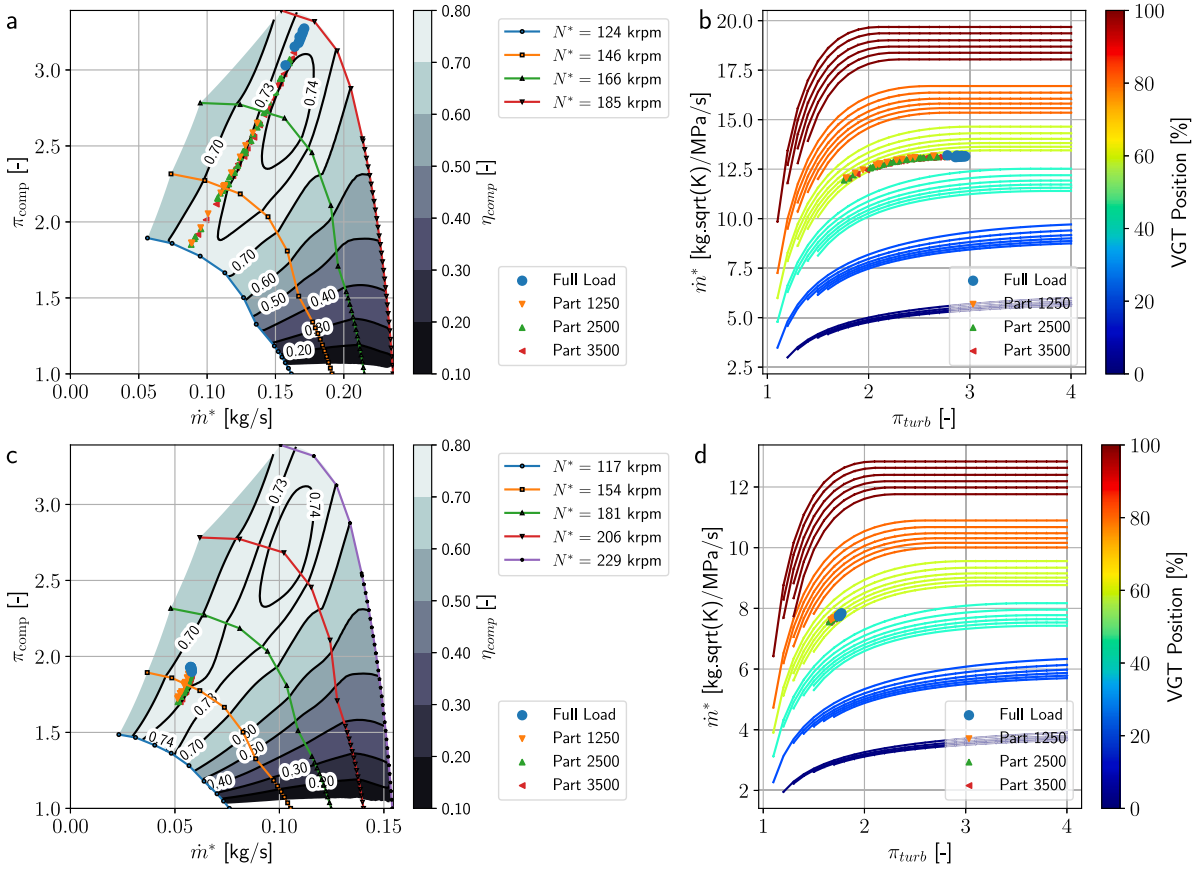

Fig. 11. Turbochargers maps: VGT NA-1 (Compressor a and Turbine b), VGT NA-2 (Compressor c and Turbine d) and VGT GO (Compressor e and Turbine f).

beforehand such as: mass flow of oxygen generated by the membrane ($\dot{m}_{O_2}$ in kg s^{-1}), cooling power at cooler C-1 (Q_{C-1} in kW), flow sensible enthalpies at MIEC feed side and system air inlets ($H_{air,in,MIEC}$ and $H_{air,in,system}$ respectively in kW), heat released by combustion (HR in kW), brake power (W in kW) and convective heat losses at cylinder walls and exhaust pipes (Q_{htw} and Q_{pipes} respectively in kW). Afterwards, total thermal energy transferred to air from system entry until MIEC feed side inlet ($H_{MIEC,real}$ in kW), mass flow of oxygen generated by membrane per engine cycle ($\dot{m}^*_{O_2}$) and analysis variables (*parameter* 1, *parameter* 2, *parameter* 1* and *parameter* 2*) may be defined as follows:

$$\dot{m}^*_{O_2}\ [\mathrm{g/cycle}] = \frac{\dot{m}_{O_2}\ [\mathrm{kg\,s^{-1}}] \times 2 \times 60 \times 1000}{Engine\ Speed\ [\mathrm{rpm}]} \tag{2}$$

$$H_{MIEC,real}\ [\mathrm{kW}] = H_{air,in,MIEC} - H_{air,in,system} + Q_{C-1} \tag{3}$$

$$parameter\ 1\ [-] = \frac{H_{MIEC,real}}{HR} \tag{4}$$

$$parameter\ 2\ [-] = \frac{H_{MIEC,real}}{HR - W - Q_{htw} - Q_{pipes}} \tag{5}$$

$$parameter\ 1^*\ [\mathrm{g/cycle}] = \frac{\dot{m}^*_{O_2}}{parameter\ 1} \tag{6}$$

$$parameter\ 2^*\ [\mathrm{g/cycle}] = \frac{\dot{m}^*_{O_2}}{parameter\ 2} \tag{7}$$

Parameters 1 and 2 present a ratio of the required energy for producing necessary oxygen by MIEC with respect to fuel caloric value and exhaust gas available thermal energy, respectively. The denominator of parameter 2 is an energy balance between the intake manifold and exhaust pipes considering major heat losses and mechanical power released, and consequently, it measures the gas enthalpy leap surrounding cylinders. Parameters 1* and 2* are basically parameters 1 and 2, respectively, taking into account the amount of generated oxygen per four-stroke cycle. Their values can be read as how much energy is needed in the MIEC to produce 1 g of oxygen per four-stroke engine cycle, and with respect to either the energy released in the fuel (parameter 1*) or delivered by the exhaust gases (parameter 2*).

Attention should be drawn to the fact that many parameters were studied but the ones depicted here seem to be the most representative for analyzing engine part-load conditions. Fig. 15 shows how parameter 1 is not reliant on neither engine speed nor load degree. By contrast, parameter 1* follows the power reduction trend with almost constant values on iso-load lines, and, besides that, it tends to a minimum value around 1 from which load may not be decreased regardless of engine speed. One may interpret parameter 1* as how many times HR must be greater than $H_{MIEC,real}$ for producing 1 g/cycle of oxygen, and those limit values observed on maps show that HR must be at least equal to $H_{MIEC,real}$ in order to ensure suitable thermal-energy availability for oxygen generation of 1 g/cycle. If that value is still lower to produce every gram of oxygen per four-stroke engine cycle, it would not be enough with just recovering the waste energy of the exhaust gases. Therefore, more energy should be added to have a self-sustaining stable system. Parameter 1* it is a very simple parameter, which can be used for design purposes as a priori parameter, that allows scaling up the whole system to any membrane and 4-stroke engine cycle.

A similar observation is verified in Fig. 16 whereby no clear trend is found for parameter 2, and parameter 2* is almost steady concerning the same engine load points. In this case, parameter 2* may be interpreted as how many times gas enthalpy increment must be greater than $H_{MIEC,real}$ for producing 1 g/cycle of oxygen, and their values tend to a minimum one around 0.5 independent of engine speed. In addition, that smallest value indicates that gas enthalpy gain must be at least half the $H_{MIEC,real}$ to guarantee proper MIEC thermal conditions for 1 g/cycle oxygen production just recovering waste energy from the

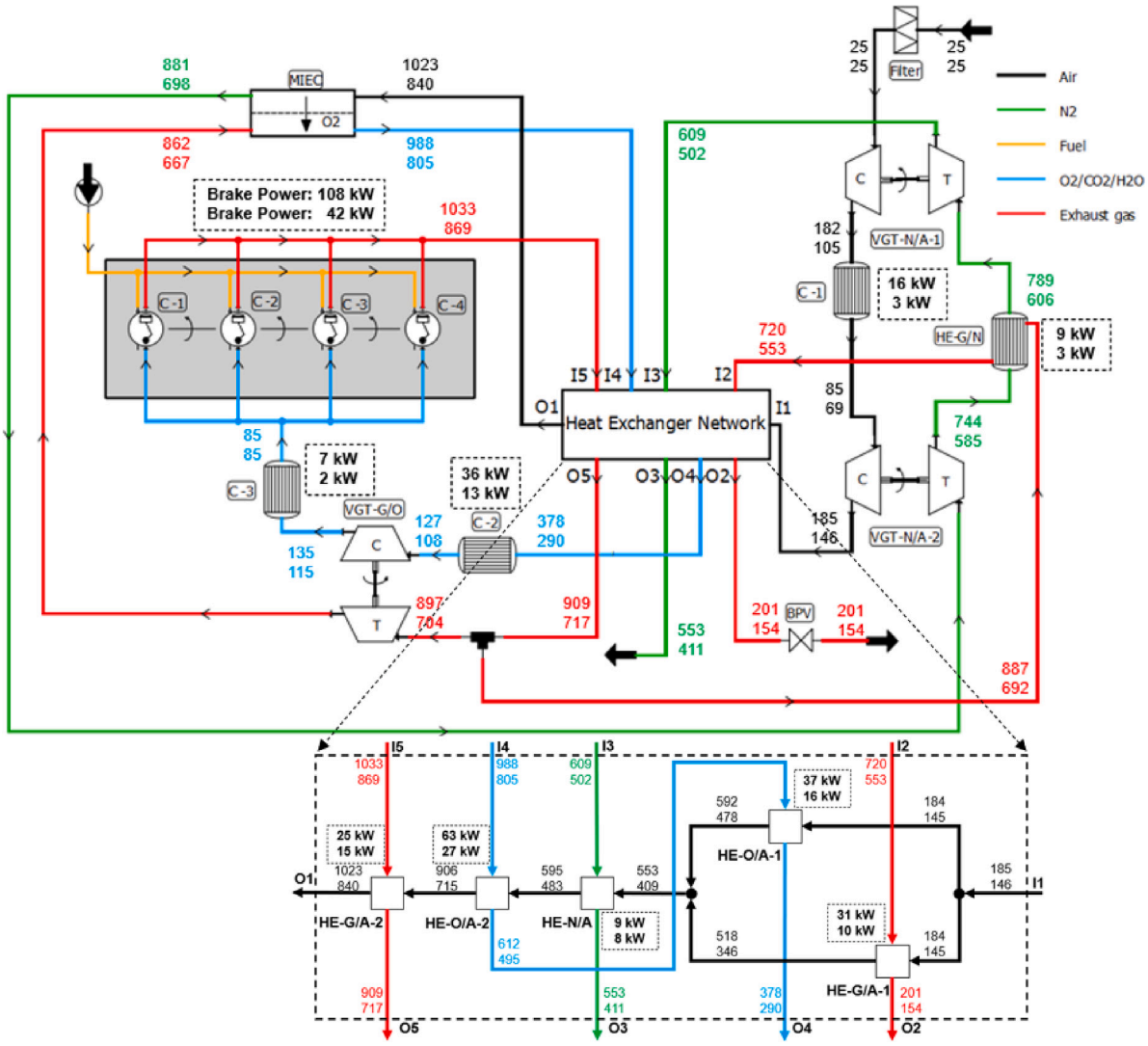

Fig. 12. Power (in kW) and temperature (in °C) distribution diagram at 2500 rpm for full-load point (top values) and 40% part-load point (bottom values).

exhaust gases. The value is lower than 1 due to the regenerative cycle behavior and the virtuous cycle effect caused by the HEs.

Thus, if parameters 1* and 2* present values lesser than the minimum ones already explained, the regenerative process would not be enough to maintain engine stability, and oxygen should be provided by an external source apart from the membrane. Finally, parameter 2* may be useful for analysis since it considers the effective enthalpy increment necessary for appropriate MIEC operating conditions. In contrast, parameter 1* may be employed for system design since fuel calorific value is commonly known and may be used to estimate MIEC oxygen production capacity and membrane minimum mass-transfer area.

4. Conclusions

A strategy is proposed to extend the load operation map range of a compression ignition engine (CIE) under oxy-fuel combustion conditions using a mixed ionic-electronic conducting membrane (MIEC) to separate oxygen from the air, enabling upcoming CO_2 capture and preventing NO_x emissions. The strategy consists basically of modifying exhaust gas temperature (T_{exh}) and oxygen-fuel ratio (λ), generating temperature-lambda maps to decide the optimal load reduction combination in terms of engine performance at 1250 rpm, 2500 rpm and 3500 rpm actuating on start of injection.

There is a minimum consumption zone on those maps wherein the benefits of low exhaust temperature are observed due to less convective heat losses and more excess of oxygen that improves combustion performance. In those cases, if compared to the corresponding full-load point, a brake specific fuel consumption enhancement is seen, around 6.2%, 6.8% and 7.5% for 1250 rpm, 2500 rpm and 3500 rpm respectively. For those engine speeds, minimum-consumption paths are proposed combining T_{exh} and λ, and a similar procedure may be carried out to extend this methodology towards other engine speeds. In addition, a minimum ignition pressure around 40 bar is found to trigger combustion with ignition temperature around 550 °C, establishing limits of combustion feasibility regardless of in-cylinder oxygen content.

Comparing a full-load point with a 40% load one at the same engine speed, one may see a reduction of heat exchanged over several heat exchangers for the part-load case due to less exhaust gas heat generated by combustion. Indeed, a decline in energy availability decreases air mass flow and MIEC feed side pressure boosted by nitrogen variable geometry turbochargers because the system is based on a regenerative process. Thus, reductions of up to around 50% in heat exchanged in HEs decrease pressure and mass flow by half over the system different parts.

Finally, four parameters are proposed to analyze system stability in terms of combustion energy availability for generating oxygen and finding out oxy-fuel engine operation limits. On the one hand, Parameter

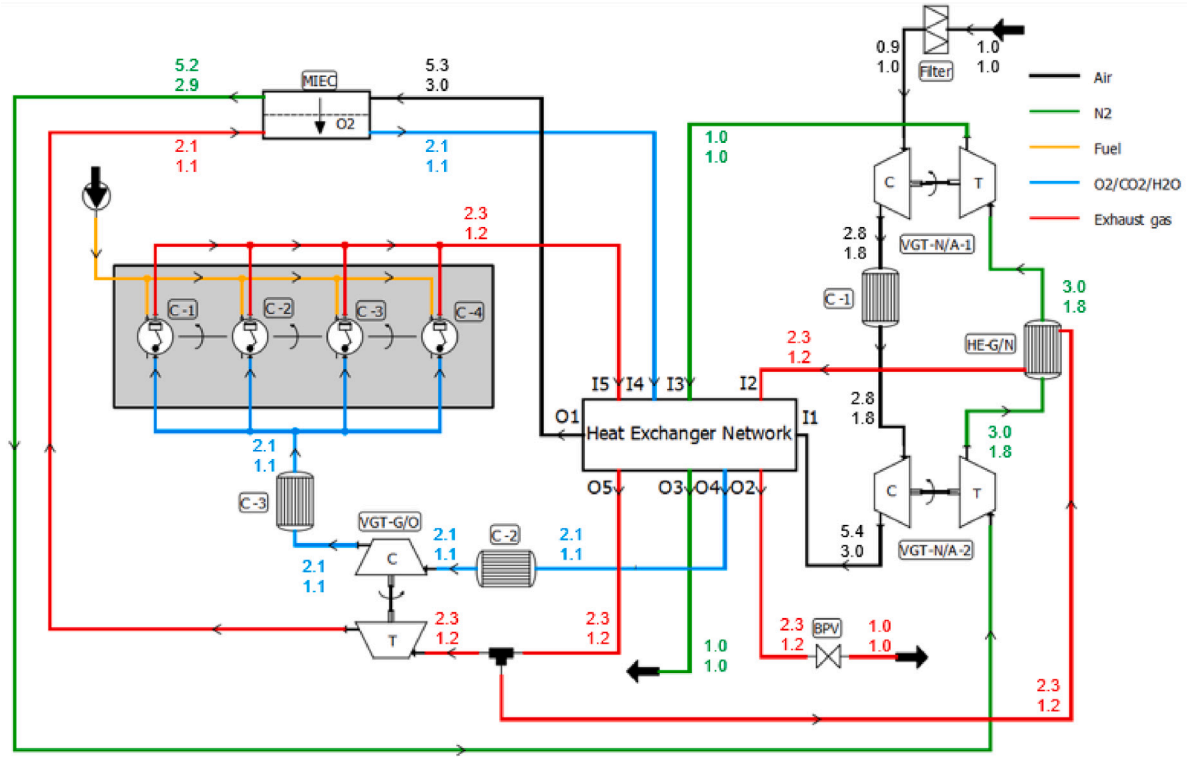

Fig. 13. Pressure (in bar) distribution diagram at 2500 rpm for full-load point (top values) and 40% part-load point (bottom values).

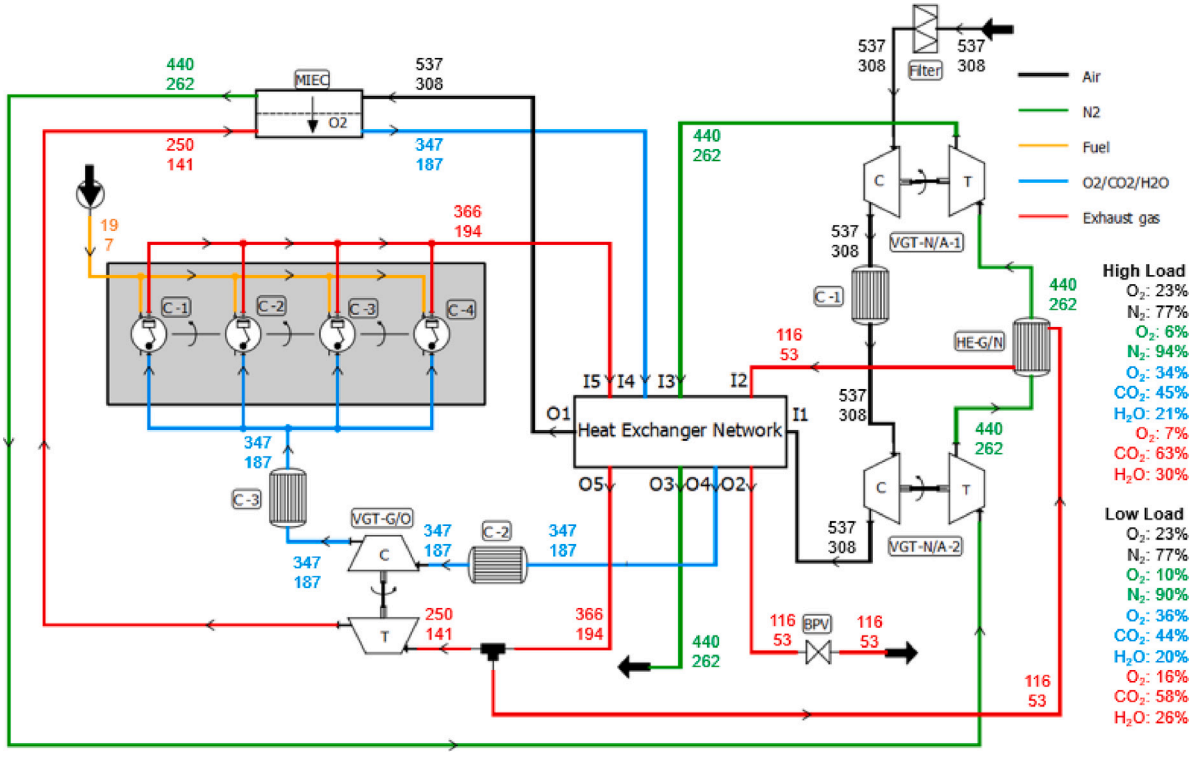

Fig. 14. Mass flow (in $kg\,h^{-1}$) distribution diagram at 2500 rpm for full-load point (top values) and 40% part-load point (bottom values).

1* may be employed for system design since fuel calorific value is commonly known and may be used to estimate MIEC oxygen production capacity and membrane design features such as minimum mass-transfer area depending on MIEC energy requirements. On the other hand, Parameter 2* may be useful for analyzing suitable energy distribution since it takes into account the energy balance surrounding cylinders to calculate the outlet and inlet sensible enthalpy difference necessary for MIEC proper oxygen generation. Parameter 1* and Parameter 2* tend to have a minimum value of 1 and 0.5, respectively, from which a decrease in engine load is not possible. Accordingly, the minimum value

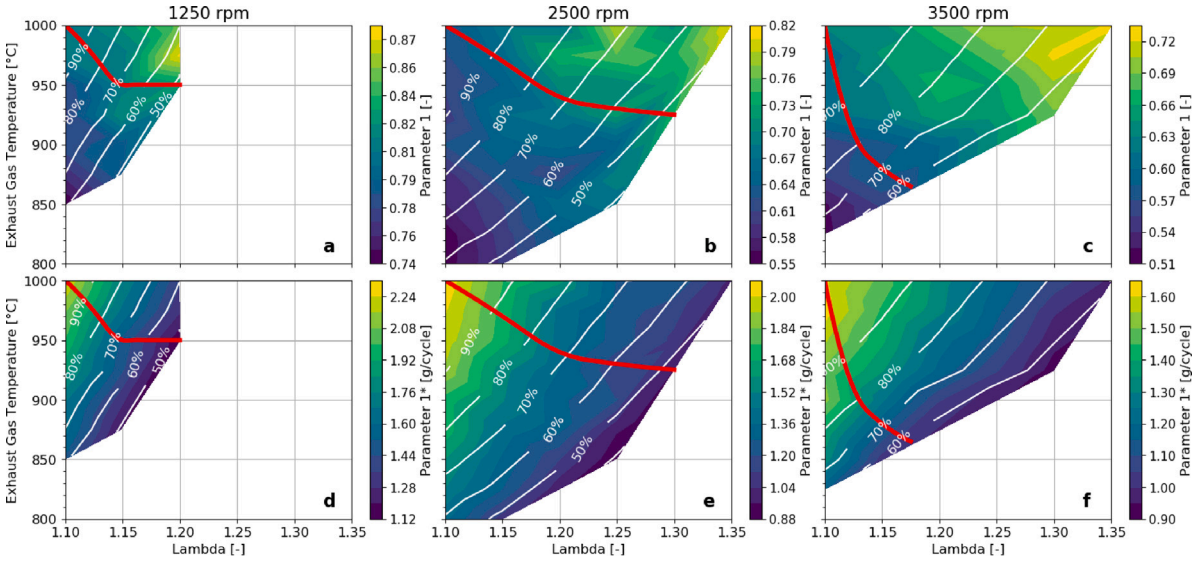

Fig. 15. Part-load maps for average results of parameter 1 for 1250 rpm, 2500 rpm and 3500 rpm. The white lines drawn on maps represent level curve for degree of engine load relative to maximum power achieved at corresponding engine speed.

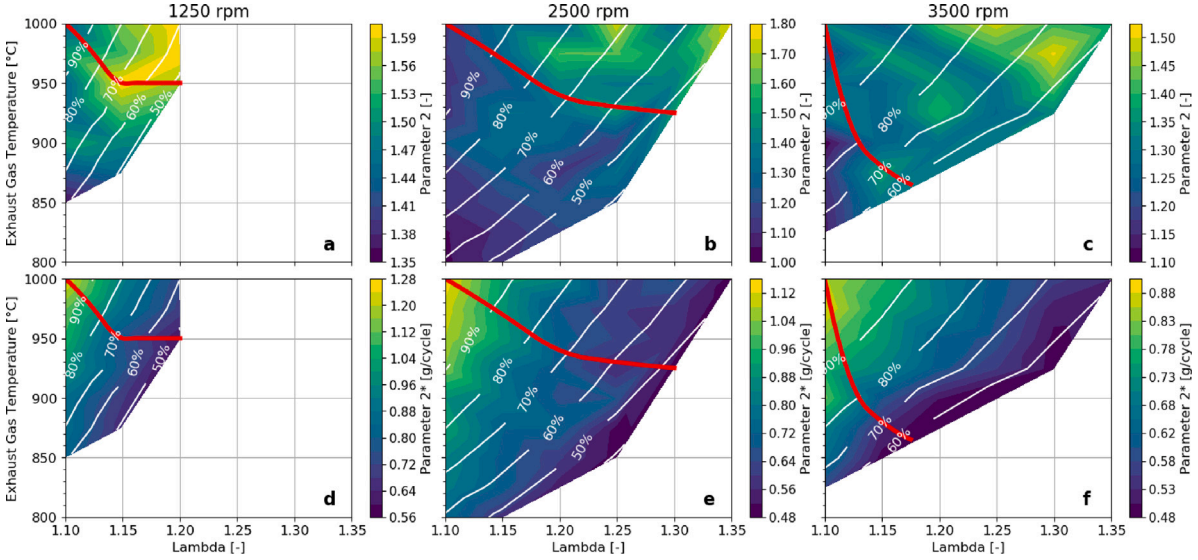

Fig. 16. Part-load maps for average results of parameter 2 for 1250 rpm, 2500 rpm and 3500 rpm. The white lines drawn on maps represent the level curve for the degree of engine load relative to maximum power achieved at corresponding engine speed.

of engine load achieved in this proposed oxy-fuel layout is around 50% considering 1250 rpm, 2500 rpm and 3500 rpm. At last, this manuscript is the first work in the literature in which a multi-cylinder CIE with oxy-fuel combustion and in-situ oxygen self-generation is studied under part-load conditions.

Declaration of competing interest

The authors declare the following financial interests/personal relationships which may be considered as potential competing interests: Vitor Hugo Farias reports financial support was provided by Government of Valencia.

Data availability

No data was used for the research described in the article.

Acknowledgments

This work has been partially supported by Grant PID2021-123351OB-I00 funded by MCIN/AEI/10.13039/501100011033 and, as appropriate, by "ERDF A way of making Europe" and by Grant CIPROM/2021/061 funded by Generalitat Valenciana, Spain. In addition, this work has been also partially founded by Universitat Politècnica de València, Spain (UPV-SOLGEN-7967) and Generalitat Valenciana, Spain (GRISOLIAP/2020/078).

References

[1] M. Rahimi, Public awareness: What climate change scientists should consider, Sustainability 12 (20) (2020) 8369, http://dx.doi.org/10.3390/su12208369.
[2] E. Commission, 2030 climate and energy framework in European Union, https://ec.europa.eu/clima/policies/strategies/2030_en.
[3] E. Commission, A European strategy for low-emission mobility, https://ec.europa.eu/clima/policies/transport_en#tab-0-0.

[4] E.E. Agency, Greenhouse gas emissions from transport in Europe, https://www.eea.europa.eu/ims/greenhouse-gas-emissions-from-transport.

[5] R. Babayev, A. Andersson, A. Dalmau, H. Im, B. Johansson, Computational optimization of a hydrogen direct-injection compression-ignition engine for jet mixing dominated nonpremixed combustion, Int. J. Engine Res. 23 (5) (2021) 754–768, http://dx.doi.org/10.1177/14680874211053556.

[6] M.S. Wooldridge, R. Singh, L.G. Gutierrez, S. Clancy, Survey of strategies to reduce cold-start particulate, CO, NO_x, and hydrocarbon emissions from direct-injection spark-ignition engines, Int. J. Engine Res. (2022) 14680874211068576, http://dx.doi.org/10.1177/14680874211068576.

[7] J. Pastor, J. Garcia-Oliver, C. Micó, A. Garcia, An experimental study with renewable fuels using ECN spray A and D nozzles, Int. J. Engine Res. 23 (10) (2021) 146808742110312, http://dx.doi.org/10.1177/14680874211031200.

[8] B. Metz, O. Davidson, P. Bosch, E. al, IPCC AR4. Climate change 2007: Mitigation. Contribution of working group III to the fourth assessment report of the intergovernmental panel on climate change, in: Climate Change 2007: The Physical Science Basis, Vol. 4, 2007.

[9] R. Mobasheri, A. Abdel, Z. Peng, X. Li, A numerical study of the effects of oxy-fuel combustion under homogeneous charge compression ignition, Int. J. Engine Res. 23 (4) (2021) 649–660, http://dx.doi.org/10.1177/1468087421993359.

[10] M. Pamminger, W. Buyu, C. Hall, R. Vojtech, T. Wallner, The impact of water injection and exhaust gas recirculation on combustion and emissions in a heavy-duty compression ignition engine operated on diesel and gasoline, Int. J. Engine Res. 21 (2019) 1555–1573, http://dx.doi.org/10.1177/1468087418815290.

[11] Z. Chen, X. Zhang, W. Luo, J. Guo, Z. Tai, P. Li, Z. Liu, Dynamic modeling on the mode switching strategy of a 35 mwth oxy-fuel combustion pilot plant, Energy Fuels 34 (2) (2020) 2260–2271, http://dx.doi.org/10.1021/acs.energyfuels.9b02968.

[12] D. Hanak, D. Powell, V. Manovic, Techno-economic analysis of oxy-combustion coal-fired power plant with cryogenic oxygen storage, Appl. Energy 191 (2017) 193–203, http://dx.doi.org/10.1016/j.apenergy.2017.01.049.

[13] X. Wei, V. Manovic, D. Hanak, Techno-economic assessment of coal-or biomass-fired oxy-combustion power plants with supercritical carbon dioxide cycle, Energy Convers. Manage. 221 (2020) 113143, http://dx.doi.org/10.1016/j.enconman.2020.113143.

[14] J. Guo, Z. Liu, X. Huang, T. Zhang, W. Luo, F. Hu, P. Li, C. Zheng, Experimental and numerical investigations on oxy-coal combustion in a 35mw large pilot boiler, Fuel 187 (2017) 315–327, http://dx.doi.org/10.1016/j.fuel.2016.09.070.

[15] F. Hu, P. Li, W. Li, C. Ding, J. Guo, Z. Liu, Experimental and kinetic study of NO-reburning by syngas under high CO2 concentration in a jet stirred reactor, Fuel 304 (2021) 121403, http://dx.doi.org/10.1016/j.fuel.2021.121403.

[16] F. Carrasco Maldonado, R. Spörl, K. Fleiger, V. Hoenig, J. Maier, G. Scheffknecht, Oxy-fuel combustion technology for cement production - state of the art research and technology development, Int. J. Greenh. Gas Control 45 (2016) 189–199, http://dx.doi.org/10.1016/j.ijggc.2015.12.014.

[17] A. Escudero, S. Espatolero, L. Romeo, Oxy-combustion power plant integration in an oil refinery to reduce CO2 emissions, Int. J. Greenh. Gas Control 45 (2016) 118–129, http://dx.doi.org/10.1016/j.ijggc.2015.12.018.

[18] X. Li, Z. Peng, Y. Pei, T. Ajmal, K.-J. Rana, A. Aitouche, R. Mobasheri, Oxy-fuel combustion for carbon capture and storage in internal combustion engines – A review, Int. J. Energy Res. 46 (2) (2021) 505–522, http://dx.doi.org/10.1002/er.7199.

[19] X. Li, Y. Pei, Z. Peng, T. Ajmal, K.-J. Rana, A. Aitouche, R. Mobasheri, Numerical study on the effects of intake charge on oxy-fuel combustion in a dual-injection spark ignition engine at economical oxygen-fuel ratios, Int. J. Engine Res. 23 (9) (2021) 1602–1616, http://dx.doi.org/10.1177/14680874211022292.

[20] I. Mohsin, T. Al-Attas, K. Sumon, J. Bergerson, S. McCoy, M. Kibria, Economic and environmental assessment of integrated carbon capture and utilization, Cell Rep. Phys. Sci. 1 (2020) 100104, http://dx.doi.org/10.1016/j.xcrp.2020.100104.

[21] A. Osman, Feasibility study of a novel combustion cycle involving oxygen and water, SAE Tech. Pap. (2009) 1–14, http://dx.doi.org/10.4271/2009-01-2808.

[22] J.R. Serrano, J. Martín, J. Gomez-Soriano, R. Raggi, Theoretical and experimental evaluation of the spark-ignition premixed oxy-fuel combustion concept for future CO2 captive powerplants, Energy Convers. Manage. 244 (2021) 114498, http://dx.doi.org/10.1016/j.enconman.2021.114498.

[23] Z. Kang, Z. Wu, Z. Zhang, J. Deng, Z. Hu, L. Li, Study of the combustion characteristics of a HCCI engine coupled with oxy-fuel combustion mode, SAE Int. J. Engines 10 (2017) 908–916, http://dx.doi.org/10.4271/2017-01-0649.

[24] Z. Kang, S. Chen, Z. Wu, J. Deng, Z. Hu, L. Li, Simulation study of water injection strategy in improving cycle efficiency based on a novel compression ignition oxy-fuel combustion engine, SAE Int. J. Engines 11 (6) (2018) 935–945, http://dx.doi.org/10.4271/2018-01-0894.

[25] H.-W. Wu, R.-H. Wang, Y.-C. Chen, D.-J. Ou, T.-Y. Chen, Influence of port-inducted ethanol or gasoline on combustion and emission of a closed cycle diesel engine, Energy 64 (2014) 259–267, http://dx.doi.org/10.1016/j.energy.2013.11.027.

[26] L. Fu, Z. Wu, L. Li, X. Yu, Effect of water injection temperature on characteristics of combustion and emissions for internal combustion rankine cycle engine, SAE Tech. Pap. 2014 (2014) http://dx.doi.org/10.4271/2014-01-2600.

[27] R. Shaw, H. Oman, Non-air working fluids for closed-cycle diesel engines, in: Inter-Society Energy Conversion Engineering Conference, The Boeing Company, 1983.

[28] N. Mancini, A. Mitsos, Conceptual design and analysis of ITM oxy-combustion power cycles, Phys. Chem. Chem. Phys. : PCCP 13 (2011) 21351–21361, http://dx.doi.org/10.1039/c1cp23027a.

[29] E. Portillo, B. Alonso-Fariñas, F. Vega, M. Cano, B. Navarrete, Alternatives for oxygen-selective membrane systems and their integration into the oxy-fuel combustion process: A review, Sep. Purif. Technol. 229 (2019) 115708, http://dx.doi.org/10.1016/j.seppur.2019.115708.

[30] F. Wu, M. Argyle, P. Dellenback, M. Fan, Progress in O2 separation for oxy-fuel combustion – A promising way for cost-effective CO2 capture: A review, Prog. Energy Combust. Sci. 67 (2018) 188–205, http://dx.doi.org/10.1016/j.pecs.2018.01.004.

[31] S. Baumann, J. Serra, M. Lobera, S. Escolástico, F. Schulze-Kuppers, W. Meulenberg, Ultrahigh oxygen permeation flux through supported $Ba_{0.5}Sr_{0.5}Co_{0.8}Fe_{0.2}O_3$-$\delta$ membranes, J. Membr. Sci. 377 (2011) 198–205, http://dx.doi.org/10.1016/j.memsci.2011.04.050.

[32] D. Catalán Martínez, M. Santafé-Moros, J. Gozálvez-Zafrilla, J. García Fayos, J. Serra, Characterization of oxygen transport phenomena on BSCF membranes assisted by fluid dynamic simulations including surface exchange, Chem. Eng. J. 387 (2020) 124069, http://dx.doi.org/10.1016/j.cej.2020.124069.

[33] M. Balaguer, C. Solís, J. García Fayos, E. Palafox, J. Serra, Progress in $Ce_{0.8}Gd_{0.2}O_2$-δ protective layers for improving the CO2 stability of BSCF O2-transport membranes, Sustain. Energy Fuels 4 (2020) 3747–3752, http://dx.doi.org/10.1039/D0SE00324G.

[34] C. Solís, F. Toldrá Reig, M. Balaguer, S. Somacescu, J. García Fayos, E. Palafox, J. Serra, Mixed ionic-electronic conduction in $NiFe_2O4 - Ce_{0.8}Gd_{0.2}O_2$-$\delta$ nanocomposite thin films for oxygen separation, ChemSusChem 11 (2018) 2818–2827, http://dx.doi.org/10.1002/cssc.201800420.

[35] F.J. Arnau, J. Benajes, J. Desantes, J.R. Serrano, J. Serra, D. Catalán-Martínez, L. García-Cuevas, Motor de combustión interna de hidrocarburos auto transportable que no emite gases nocivos ni CO2; secuestra CO2 atmosférico y fabrica CO2 líquido subcrítico, 2019, P201930285.

[36] J.R. Serrano, F.J. Arnau, L. García-Cuevas, V.H. Farias, Oxy-fuel combustion feasibility of compression ignition engines using oxygen separation membranes for enabling carbon dioxide capture, Energy Convers. Manage. 247 (2021) 114732, http://dx.doi.org/10.1016/j.enconman.2021.114732.

[37] J. Arrègle, J.J. López, J.M. García, C. Fenollosa, Development of a zero-dimensional diesel combustion model. Part 1: Analysis of the quasi-steady diffusion combustion phase, Appl. Therm. Eng. 23 (11) (2003) 1301–1317, http://dx.doi.org/10.1016/S1359-4311(03)00079-6.

[38] J. Arrègle, J.J. López, J.M. García, C. Fenollosa, Development of a zero-dimensional diesel combustion model: Part 2: Analysis of the transient initial and final diffusion combustion phases, Appl. Therm. Eng. 23 (11) (2003) 1319–1331, http://dx.doi.org/10.1016/S1359-4311(03)00080-2.

[39] J. Arrègle, J.J. López, J. Martín, E.M. Mocholí, Development of a mixing and combustion zero-dimensional model for diesel engines, SAE Tech. Pap. (2006) 1381, http://dx.doi.org/10.4271/2006-01-1382.

[40] J. Martín, F.J. Arnau, P. Piqueras, A. Auñón, Development of an integrated virtual engine model to simulate new standard testing cycles, SAE Tech. Pap. 2018-April (2018) 1413, http://dx.doi.org/10.4271/2018-01-1413.

[41] F. Payri, F.J. Arnau, P. Piqueras, M. Ruiz, Lumped approach for flow-through and wall-flow monolithic reactors modelling for real-time automotive applications, in: SAE International, 2018, http://dx.doi.org/10.4271/2018-01-0954.

[42] J.R. Serrano, G. Bracho, J. Gomez-Soriano, C. Spohr Fernandes, Development of an oxy-fuel combustion system in a compression-ignition engine for ultra-low emissions powerplants using CFD and evolutionary algorithms, Appl. Sci. 12 (14) (2022) 7104, http://dx.doi.org/10.3390/app12147104.